



**LABEL-FREE GOLD INTERDIGITATED
MICROELECTRODES IMMUNOSENSOR FOR
PROSTATE CANCER BIOMARKER**

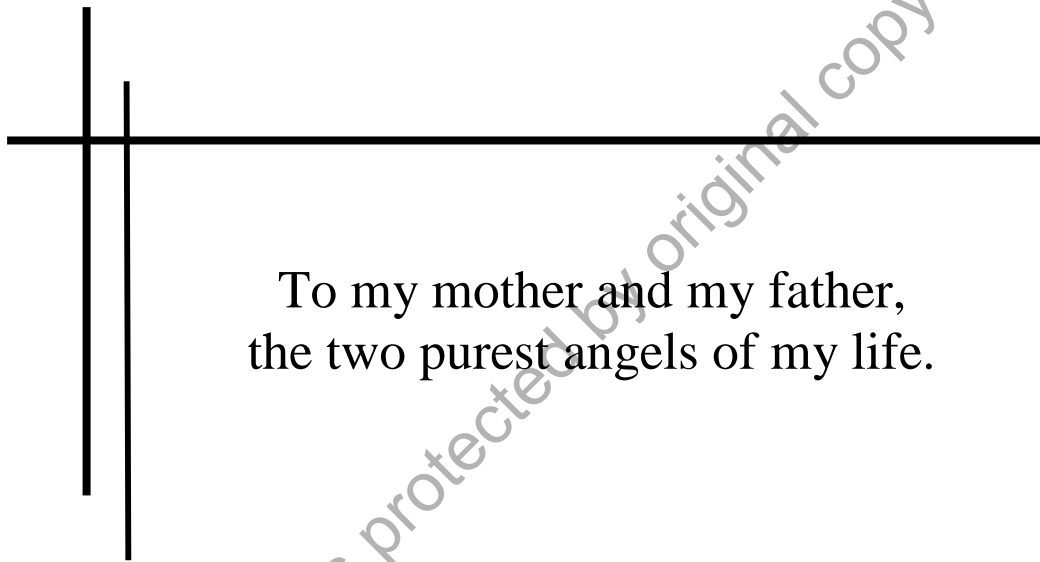
by

**Conlathan Ibau
(1641712193)**

A thesis submitted in fulfillment of the requirements for the degree of
Doctor of Philosophy

**Institute of Nano Electronic Engineering
UNIVERSITI MALAYSIA PERLIS**

2020



To my mother and my father,
the two purest angels of my life.

©This item is protected by original copyright

ACKNOWLEDGMENT

To travel on such an ‘eventful’ PhD journey, one couldn’t possibly withstand it all without the supports from his loved ones. Likewise, I am very fortunate to be blessed with a supportive family who has never hesitate nor doubtful of my capabilities and choices. I would love to take this opportunity to bid my sincerest gratitude for having them, to the most beautiful woman in my life, my mother, Kylin I Choon and my father, Ibau Din Lean, for not being just the pillar of support throughout these entire adventures, but also for being who they really are, simply a pair of loving parents. Not to be forgotten, to my beloved elder brother, Phaisol Ibau for wielding such a diligence and caring personalities, and his trusts unto this little brother have enabled countless possibilities. To his wife, Champi Khun for the delicious home-cooks, and to my two beautiful little monkeys, my nieces, Mischa Daren and Nischa Daren who have always brighten my days whenever I’m home. Oh, and also to Percy, my beautiful koi pond who has been there whenever I need some doses of tranquility.

The next person I would like to share my utmost gratitude with is my PhD advisor, Associate Professor Ir. Dr. Mohd Khairuddin Md Arshad, a man who made the impossible possible. Although sometimes, we are like Tom and Jerry, and it’s very obvious who’s Tom here, I am much honored to have a caring and attentive advisor such as him. His dedication and supports are unrivalled, and I am lucky enough to have this learning opportunity under his guidance. We have secured two research grants together, The Newton-Ungku Omar Grant 2017 and Majlis Kanser Nasional (MAKNA) Cancer Research Grant 2017 that have embarked for much more exciting learning curve over these past years. I am whole-heartedly grateful for all these chances and experiences shared, not to be forgotten the one during our mobility program in the University of Bath, United Kingdom while looking for an accommodation in the winter of February 2017. That was my first snow experience too. Thank you!

The next most impactful persons during this journey are both of my co-advisors, Associate Professor Dr. Subash Bose Gopinath and Associate Professor Dr. Mohammad Nuzaihan Md Nor. I would like to convey my utmost gratitude towards them for their advices, technical discussions and proof-reading of my manuscripts. Congratulations to Dr. Mohammad Nuzaihan Md Nor on his recent promotion to an Associate Professor.

A special thank you to the Director of the Institute of Nano Electronic Engineering, Associate Professor Dr. Ruslinda A. Rahim for providing the facilities and knowledge sharing. Her leadership in INEE is something to take note of. My deepest gratitude to all INEE researchers as well, to Dr. Nur Hamidah Abdul Halim, Dr. Mohamad Faris Mohamad Fathil, Dr. Nor Azizah Parmin, Dr. Foo Kai Loong, Dr. Ramzan Mat Ayub, Dr. Liu Wei Wen, and Dr. Voon Chun Hong for their technical supports.

No man is an island. I couldn’t have possibly reached this point without the warm supports and helping hands of the Nanorians family members. To name a few,

Dr. Fatin Nabilah, Dr. Shahidah, Dr. Asanka and his wife, Malithi, Dr. Siti Fatimah, Miss Dalila ‘Dinda Lala’, Miss Thivina ‘Miss Divine’, Miss Khairun ‘Khai of Padbara’, Miss Adilah of Penn State, Mr. Azrul ‘my bae’, Miss Atiqah the ‘MCB-GBKN’, Mr. Steven Taniselas, Miss Syifa, Mr. Adzhri, Miss Huda, Mr. Lee, Mr. Zaki, Miss Adelyn Puah, Mr. Lam, Mr. Azman, Mrs Farehanim, Mr. Iman, Mr. Suhaimi. All those thick and thin that we went through together, to name some, all those delicious bowls of ‘*Maggi Kari tambah telur*’ coupled with countless hours of Blockbuster movies during our free time was simply the most memorable moments throughout this journey. To my ‘homie’ buddies, Chan Tian Seng, Khairul Anuar, Jimmy Tan Chun Hao and Lai Siang Leng, congratulations on your thesis submission and thank you for sharing such a great friendship all these years.

Next, special dedication to my lecturers who are also my friends, Mr. Hafiz Ismail and Dr. Nurjuliana Juhari who have taught me since my Diploma days in UniMAP and have been there since for the much needed emotional supports, couple rounds of tennis and badminton, the so-called our effective ‘de-stress therapies’, and perhaps, for another couple of plates of free-of-charge “Hanna Cookies”. Thank you for just being there.

I would also like to extend my appreciation to the laboratory staffs, all in the Institute of Nano Electronic Engineering, Micro-fabrication Cleanroom in the School of Microelectronic Engineering, and also in AMBIENCE, UniMAP. Special mentions to Mr. Jasni, our dedicated lab manager, our late technician, Mr. Ijat who although had passed away but his legacy in our lab shall be remembered for years to come. Notable mentions to Mrs. Mira, Mrs. Rozaini, Mrs. Rohaiza, Mr. Syed Fais and Mr. Roy for their administrative supports. My appreciations are further extended to Mr. Bahari Man and Mr. Muhamad Nasir Bakar, both are very helpful and knowledgeable technicians who have impactful contributions to the success of this research.

I am truly honored to be awarded with a scholarship and two research grants, and thus would like to grab this opportunity to thank the following organizations. I would like to extend my deepest appreciation to the Ministry of Higher Education, Malaysia for funding me with MyBrain15 scholarship for the past 3 years. Moreover, I am very thankful to The Academy of Science, Malaysia for awarding me with Majlis Kanser Nasional (MAKNA) Cancer Research Award 2017 and co-awarded the prestigious Newton-Ungku Omar Grant 2017 with my advisor that has enabled us the golden opportunity for an exchange program in the University of Bath, United Kingdom. Not to be forgotten, many thanks to Professor Dr. Pedro Estrela, my co-advisor in the University of Bath, and to other ‘lab-mates’ in the Centre for Biosensors, Bioelectronics and Biodevices (C3Bio) and Department of Electronic & Electrical Engineering, University of Bath, with a notable mention to my tennis and travelling buddy, Domingos de la Costa for our great tennis runs while we were at Bath.

Last but not the least, I thank myself who have persevered through it all, who is blessed with an amazing family, buddies and colleagues, and who has cherished every second of this insightful journey which had vastly broaden his knowledge and experience.

[Click here to enter text.](#)

TABLE OF CONTENTS

	PAGE
DECLARATION OF THESIS	i
ACKNOWLEDGMENT	iii
TABLE OF CONTENTS	v
LIST OF TABLES	ix
LIST OF FIGURES	x
LIST OF ABBREVIATIONS	xv
LIST OF SYMBOLS	xviii
ABSTRAK	xx
ABSTRACT	xxii
CHAPTER 1 : INTRODUCTION	1
1.1 Motivation	1
1.2 Research background	2
1.3 Problem statement	4
1.4 Research objectives	5
1.5 Research scopes	6
1.6 Thesis organization	8
CHAPTER 2 : LITERATURE REVIEW	11
2.1 Introduction	11
2.2 Prostate cancer	11
2.2.1 Candidate biomarkers	13

2.2.1.1	Prostate-specific antigen	14
2.2.1.2	Glycosylation	17
2.2.1.3	MicroRNAs	18
2.3	Electrochemical biosensor	19
2.3.1	Principle of electrochemistry	21
2.3.2	Electrochemical Impedance Spectroscopy	25
2.4	Review on PSA detection methods using customized-electrodes devices	34
2.4.1	Interdigitated microelectrodes	37
2.4.2	Screen-printed electrodes	39
2.4.3	Glassy carbon electrodes	41
2.5	Summary	47
CHAPTER 3 : METHODOLOGY		49
3.1	Introduction	49
3.2	Overall process flow	49
3.3	Fabrication of ID μ E biosensor	51
3.3.1	Materials and reagents	51
3.3.2	Mask design	53
3.3.3	Single-masking fabrication process of ID μ E biosensor	54
3.3.4	ID μ E device cleaning	58
3.4	Anti-PSA probe immobilization techniques	58
3.4.1	Scheme 1: Probe immobilization on SiO ₂ interdigitated gaps	60
3.4.1.1	Materials and reagents	60
3.4.1.2	SAM with amino-silanization using APTES on SiO ₂ interdigitated gaps	61
3.4.1.3	Immobilization of anti-PSA on SiO ₂ interdigitated gaps	63
3.4.2	Scheme 2: Probe immobilization on gold microelectrode	65
3.4.2.1	Materials and reagents	65

3.4.2.2	SAM with thiolation chemistry using 16-MUA on gold microelectrode surface	66
3.4.2.3	Immobilization of anti-PSA on Au microelectrode surface	67
3.5	Techniques for validating successful anti-PSA probe immobilization	68
3.5.1	Atomic force microscopy	69
3.5.2	Water contact angle measurement	70
3.5.3	X-ray photoelectron spectroscopy	71
3.5.4	Cyclic voltammetry	72
3.6	ID μ E-based EIS detection of PSA	73
3.6.1	Materials and reagents	74
3.6.2	Faradaic-EIS measurement setup	74
3.6.3	Non-Faradaic-EIS measurement setup	76
3.7	Summary	78
CHAPTER 4 : RESULTS & DISCUSSION		80
4.1	Introduction	80
4.2	Characterization of pristine ID μ E device	80
4.2.1	3-dimensional optical surface profiler	81
4.2.2	Water contact angle measurement	82
4.2.3	Scanning Electron Microscopy and Energy Dispersive Spectroscopy characterizations	83
4.3	PSA target detection using Scheme 1	85
4.3.1	Validation on successful SAM functionalization and probe immobilization	85
4.3.1.1	Water contact angle measurement	86
4.3.1.2	Atomic force microscopy	87
4.3.1.3	X-ray photoelectron spectroscopy	90
4.3.1.4	Cyclic voltammetry	93
4.3.2	Effect of changing buffers on stability of APTES-SAM layer	96
4.3.3	PSA detection by Electrochemical Impedance Spectroscopy technique	97
4.3.3.1	Impedimetric detection of PSA in Faradaic-EIS mode	97

4.3.3.2	Linear calibration curve	101
4.3.4	Sensor reproducibility study	103
4.3.5	Sensor specificity study	104
4.3.6	Sensor stability study	105
4.4	PSA target detection using Scheme 2	106
4.4.1	Validation on successful SAM functionalization and probe immobilization	107
4.4.1.1	X-ray photoelectron spectroscopy	107
4.4.2	Optimization on probe coverage on transducer surface	113
4.4.3	Effect of changing buffers on stability of 16-MUA SAM layer	115
4.4.4	PSA detection by EIS technique	116
4.4.4.1	Impedimetric detection of PSA in Faradaic-EIS mode	117
4.4.4.2	Capacitive detection of PSA in non-Faradaic EIS mode	121
4.5	PSA detection performance: Scheme 1 versus Scheme 2 assays	124
4.6	Comparison of developed sensor to other reported bioassays	125
4.7	Summary	127
	CHAPTER 5 : CONCLUSION	129
5.1	Thesis conclusion	129
5.2	Future work	131
	REFERENCES	133
	APPENDIX A	148
	APPENDIX B	150
	LIST OF PUBLICATIONS	151
	LIST OF AWARDS	155

LIST OF TABLES

		PAGE
Table 2.1	PSA biosensing techniques using customized-electrodes based devices	45
Table 3.1	Overall process flow	50
Table 3.2	List of materials and reagents used for device fabrication	52
Table 3.3	List of materials and reagents used for sensor's functionalization and probe immobilization in Scheme 1	61
Table 3.4	List of materials and reagents used for sensor's functionalization and probe immobilization in Scheme 2	65
Table 3.5	List of materials and reagents used for target binding detection using EIS measurement	74
Table 4.1	XPS spectral peaks analyses for biosensor development	113
Table 4.2	Performance comparison between developed ID μ E biosensor to other reported assays	126

LIST OF FIGURES

		PAGE
Figure 2.1	Prostate gland and prostate cancer cell (Seymour, 2019).	12
Figure 2.2	Comparison of different expression of PSA isoforms between, (i) a healthy prostate gland, and (ii) a cancerous prostate gland.	13
Figure 2.3	Stages in proliferation of PCa from a healthy prostate cell to the invasive prostate cancer cell. (a) healthy prostate gland, (b) abnormalities on luminal cells caused by various factors, (c) formation of regenerative mutated luminal cells in prostate gland, and (d) formation of cancerous cells in prostate gland.	16
Figure 2.4	Components of a biosensing platform.	21
Figure 2.5	Three-electrode electrochemical system and a depiction of electrode–electrolyte interface layer on WE.	22
Figure 2.6	Simplified circuit diagram of three-electrode electrochemical cell and potentiostat connection.	23
Figure 2.7	Charge transfer mechanism on the electrode–electrolyte interface layer of an electrochemical system.	24
Figure 2.8	Illustration of a phase angle, φ	27
Figure 2.9	Illustration of total impedance, $ Z $ and phase angle, φ in a complex plane Z'' (Ω) versus Z' (Ω).	29
Figure 2.10	Depiction of Randles equivalent circuit.	31
Figure 2.11	Nyquist plot for a Faradaic EIS system showing a semi-circular impedance response.	32

Figure 2.12	Nyquist plot for a non-Faradaic EIS system showing high impedance response.	33
Figure 2.13	Bode plot showing the relationship between capacitance values (F) versus frequency (Hz) for a non-Faradaic EIS system.	34
Figure 2.14	Example of customized-electrodes based biosensors and the commonly employed electrochemical detection techniques.	36
Figure 3.1	Chrome mask design for fabrication of ID μ E sensing device	54
Figure 3.2	Summary of ID μ E fabrication processes using a conventional lithography and ‘lift-off’ techniques, (i) wet oxidation process for SiO ₂ growth, (ii) wafer scribing, (iii) substrate cleaning process, (iv) photoresist coating and baking processes, (v) pattern transfer using conventional photolithography, (vi) photoresist development in RD6, (vii) Ti-Au metal deposition onto patterned substrate, (viii) ‘lift-off’ process, and (ix) fabricated ID μ E device for biosensing application.	57
Figure 3.3	Characteristics of ID μ E sensing surface, (i) device transducer showing both SiO ₂ and Au microelectrode, (ii) SAM modification on SiO ₂ surface (Scheme 1), and (iii) SAM modification on Au microelectrode (Scheme 2).	59
Figure 3.4	Sensing surface functionaliation steps using APTES amino-silanization chemistry on SiO ₂ interdigitated gaps. A(i) Pristine ID μ E as start-up device, A(ii) incubation of 2% APTES onto device transducer, A(iii) the amino-silanized surface using 2% APTES, B(i) methoxy (OCH ₃) head group of APTES reacting with hydroxyl (-OH) on SiO ₂ , B(ii) OCH ₃ was hydrolyzed into silanol (Si-OH), B(iii) amino-silanization on SiO ₂ through condensation process.	63
Figure 3.5	Anti-PSA immobilization on functionalized APTES-SAM layer. (i) APTES modified surface, (ii) immobilization of anti-PSA probe onto transducer surface using EDC/NHS carbodiimide crosslinker, and	

	(iii) blocking of anti-PSA unreacted sites using SB-PBS blocking agent to avoid non-specific binding event on transducer surface.	64
Figure 3.6	Sensing surface functionalization steps using 16-MUA thiolation chemistry on Au microelectrode surface. (i) Pristine device, (ii) activation of carboxyl on 16-MUA using EDC/NHS, (iii) incubation of EDC-activated 16-MUA onto Au surface, and (iv) 16-MUA thiolated Au surface.	67
Figure 3.7	Anti-PSA immobilization steps on transducer surface. (i) 16-MUA SAM layer on Au surface, (ii) anti-PSA probe immobilization, and (iii) SB-PBS blocking on anti-PSA unreacted sites to avoid non-specific binding event.	68
Figure 3.8	Atomic force microscopy equipment for morphological characterization	70
Figure 3.9	Water contact angle measurement system	71
Figure 3.10	X-ray photoelectron spectroscopy equipment	72
Figure 3.11	PGSTAT204 AUTOLAB Potentiostat for cyclic voltammogram analysis	73
Figure 3.12	Faradaic EIS measurement setup, (A) PSA target binding step, (B) PSA detection mechanism using f-EIS measurement system, and (C) three-electrode connection for f-EIS measurement setup.	76
Figure 3.13	Non-Faradaic EIS measurement setup, (A) PSA target binding step, (B) PSA detection mechanism in nf-EIS measurement system, and (C) three-electrode connection for nf-EIS measurement setup.	78
Figure 4.1	3-D optical characterization on pristine ID μ E at 20x magnification. (i) Wide 3-D imaging (133.2 nm x 177.6 nm) showing the developed Au microelectrode with maximum height (H_{max}) of 671.327 nm and average height (H_{ave}) of 334.427 nm, and (ii) narrow 3-D imaging	

	(88.8 nm x 266.4 nm) showing Au microelectrode with H_{max} of 807.402 nm and H_{ave} of 347.912 nm.	81
Figure 4.2	Water contact angle measurement on pristine ID μ E transducer surface.	83
Figure 4.3	Surface characterizations using SEM and EDS techniques. A(i) Electro-active area where SEM characterization was carried out, A(ii) SEM characterization at magnification of 100x, A(iii) SEM characterization at magnification of 1300x, B(i) electro-active area where EDS characterization was performed, and B(ii) EDS characterization data.	84
Figure 4.4	Water contact angle measurement, (i) on a pristine ID μ E surface, (ii) APTES-SAM silanized surface and (iii) successful anti-PSA probe immobilization on transducer surface.	86
Figure 4.5	AFM surface morphological study, (i) on a pristine ID μ E surface, (ii) APTES-SAM silanized surface and (iii) successful anti-PSA probe immobilization on transducer surface.	89
Figure 4.6	XPS spectral peaks analysis on ID μ E transducer surface for sensor development. A(i) Survey scan showing overall spectral peaks analysis, B(i) Si 2p narrow spectral scan, B(ii) C 1s narrow spectral scan, and B(iii) N 1s narrow spectral scan.	93
Figure 4.7	CV characterization for sensor's development. (A) CV voltammogram analysis for A(i) pristine electrode surface, A(ii) 2% APTES-SAM silanization, A(iii) anti-PSA probe immobilization, A(iv) SB-PBS blocking step. Figure B illustrates the sensors development steps	95
Figure 4.8	Effect of changing buffers on stability of APTES-SAM layer by monitoring the deviation in R_{ct} values	96
Figure 4.9	Faradaic EIS characterization for PSA binding event. (i) Nyquist plot with inset figure (a) showing Randles equivalent circuit and inset (b)	

	showing Nyquist response of pristine device. (ii) Bode plot with highest impedance change at 2.0 Hz.	100
Figure 4.10	Linear calibration curves with respect to (i) Nyquist plot and (ii) Bode plot.	102
Figure 4.11	Sensor reproducibility study showing the relative standard deviation (R.S.D) of sensors measurement.	104
Figure 4.12	Sensor's binding specificity study to discriminate HSA and hK2 non-specific targets	105
Figure 4.13	Sensor's PSA binding stability and probe density stability study	106
Figure 4.14	XPS spectral peaks analysis on ID μ E transducer surface for sensor development. (A) survey scan revealing overall spectral peaks, B(i) C 1s narrow spectral peaks, B(ii) O 1s narrow spectral peaks, B(iii) N 1s narrow spectral peaks, and B(iv) S 2p narrow spectral peaks.	111
Figure 4.15	CV voltmmogram characterization for anti-PSA probe density coverage on transducer surface	115
Figure 4.16	Effect of changing buffers on stability of 16-MUA SAM layer by monitoring the deviation in R_{ct} values	116
Figure 4.17	Impedimetric measurement for PSA detection performance in Faradaic EIS mode. (i) Nyquist plot, (ii) Bode plot and (iii) linear calibration curve for PSA detection performance of the sensor.	120
Figure 4.18	Capacitive measurement for PSA detection performance in non-Faradaic EIS mode. (i) Nyquist plot, (ii) Phase versus frequency response, (iii) Bode plot and (iv) linear calibration curve for PSA detection performance of the sensor.	124

LIST OF ABBREVIATIONS

-COOH	Carboxylic
-NH ₃ ⁺	Amine
-OH	Hydroxyl
-SH	Thiol
16-MUA	16-mercaptoundecanoic acid
AC	Alternating current
AFM	Atomic force microscopy
Anti-PSA	Prostate-specific antigen monoclonal antibody
APTES	3-aminopropyltriethoxysilane
Au	Gold
AuNPs	Gold nanoparticles
BE	Binding energy
C-C	Alkyl carbon
CE	Counter electrode
CMOS	Complementary metal-oxide semiconductor
CV	Cyclic voltammetry
DC	Direct current
DIW	De-ionized water
DNA	Deoxyribonucleic acid
DPV	Differential pulse voltammetry
DRE	Digital rectal examination
EDC	1-Ethyl-3-(3-dimethylaminopropyl)carbodiimide
EDS	Energy dispersive spectroscopy
EIS	Electrochemical Impedance Spectroscopy
eV	Electron-volts
Fc	Ferrocene
f-EIS	Faradaic-mode Electrochemical Impedance Spectroscopy
[Fe(CN) ₆] ^{4-/3-}	Ferrocyanide/ferricyanide redox
GA	Glutaraldehyde
GCE	Glassy carbon electrode
hK2	Human kallikrein 2
HPM	High power microscope

HRP	Horseradish peroxidase
HSA	Human serum albumin
Hz	Hertz
ICTS	Immunochromatography test strip
ID μ E	Interdigitated microelectrode
IPA	Isopropanol
LOD	Limit of detection
LOQ	Limit of quantification
LSV	Linear sweep voltammetry
MAb1	Monoclonal antibody 1
MAb2	Monoclonal antibody 2
MSCC	Metastatic spinal cord compression
MWCNTs	Multi-walled carbon nanotubes
nf-EIS	Non-Faradaic mode Electrochemical Impedance Spectroscopy
NHS	N-Hydroxysuccinimide
OCH ₃	Methoxy
O=C-N	Amide
OCP	Open circuit potential
PAMAM	Polyamidoamine
PAP	Prostatic acid phosphatase
PBS	Phosphate buffered saline
PCa	Prostate cancer
PEB	Post exposure bake
PtNPs	Platinum nanoparticles
PoC	Point-of-care
PSA	Prostate-specific antigen
QD	Quantum dot
RCA 1	Radio Corporation of America 1
RCA 2	Radio Corporation of America 2
RE	Reference electrode
rGO	Reduced graphene oxide
RNA	Ribonucleic acid
R.S.D	Relative standard deviation

RT	Room temperature
SAM	Self-assembled monolayer
SB-PBS	Starting Block phosphate buffered saline
scAb	Single-chain antibody
SEM	Scanning electron microscopy
Si	Silicon
SiH ₄	Silane
SiO ₂	Silicon dioxide
Si-OH	Silanol
SPE	Screen-printed electrode
SWV	Square wave voltammetry
TH	Thionine
Ti	Titanium
tPSA	Total prostate-specific antigen
PTMs	Post-translational modifications
TRUS	Transrectal ultrasound
UV	Ultraviolet
WE	Working electrode
XPS	X-ray photoelectron microscopy

©This item is protected by original copyright

LIST OF SYMBOLS

σ	Standard deviation
$\sum_{i=1}^N x_i$	Sum of all numbers of data set
ω	Angular frequency
φ	Phase angle
b	Sensor's sensitivity computed from the slope of calibration curve
C	Capacitance
c	Y-intercept
C_{CP}	Capacitance change of capture probe
C_{DL}	Double layer capacitance
C_{INS}	Capacitance change of insulating SAM layer
ΔC	Change in capacitance value
f	Frequency
F	Faraday Constant
i	Quantity of electron charges passed
I_0	Amplitude of applied current
j	Imaginary number equal to $\sqrt{-1}$
n	Rate of reaction and amount of electrons
Q	Constant phase element
R^2	Correlation coefficient
R_a	Mean surface roughness
R_{ct}	Charge transfer resistance
R_{max}	Maximum roughness
R_s	Resistance of electrolyte solution
$V(t)$	Applied voltage expressed in a function of time
V_0	Amplitude of applied voltage
Y_0	Magnitude of admittance at angular frequency = 1
Z'	Real part of impedance
Z''	Imaginary part of impedance
$ Z $	Absolute impedance
ΔZ	Change in impedance value

Z_Q	Constant phase element
Z_W	Warburg impedance

©This item is protected by original copyright

Peranti Pengesan Tindakbalas Imun Berdasarkan Interdigit Mikro-Elektrod Emas Bebas Label Untuk Penanda-Bio Barah Prostat

ABSTRAK

Barah prostat ialah sejenis barah yang merebak secara senyap dan tidak bergejala di dalam kelenjar prostat. Ia merupakan barah kedua tertinggi yang sering didiagnosis di seluruh dunia dengan catatan 28% kematian dalam kalangan pesakit. Walaupun dengan pengenalan proses saringan barah pada beberapa puluh tahun yang lalu, teknik saringan tersebut tidak mampu dicapai oleh kalangan pesakit yang tinggal di kawasan pedalaman kerana sifat proses saringan yang kompleks dan tidak mudah-alih. Pembangunan platform bio-pengesan bebas label dan mudah-alih menggunakan penanda-bio berpiawai emas seperti antigen spesifik prostat telah dilancarkan untuk menyelesaikan masalah ini, seperti mana juga dengan pembangunan peranti pengesan tindakbalas imun berdasarkan interdigit mikro-elektrod emas yang dilakukan dalam hasil kajian ini. Dalam kajian ini, peranti interdigit mikro-elektrod dipilih berdasarkan daya pengesannya yang unggul, mudah-alih dan daya pembuatan massa yang bagus. Peranti pengesan ini difabrikasi di dalam makmal menggunakan teknik fotolitografi berpiawai yang menghasilkan mikro-elektrod bersaiz $10\ \mu\text{m}$ dan jurang interdigit bersaiz $10\ \mu\text{m}$, diintegrasikan dengan elektrod kaunter emas dan elektrod rujukan samaran emas pada substrat silikon dioksida. Untuk menjadikan peranti pengesan-bio, dua skema modifikasi pada permukaan transduser dilakukan. Skema 1 melibatkan modifikasi lapisan mono terkumpul sendiri menggunakan proses 'amino-silanisasi' daripada bahan kimia 3-aminopropyltriethoxysilane dan imobilisasi antibodi monoklonal yang spesifik kepada antigen spesifik prostat di atas permukaan silikon dioksida, manakala Skema 2 menggunakan tindakbalas 'thiolasi' oleh asid 16-merkaptoundekanoik dan imobilisasi antibodinya di atas mikro-elektrod emas. Kejayaan proses modifikasi ini disahkan menggunakan teknik mikroskopi tenaga atom, pengukuran sudut hubungan air, spektroskopi fotoelektron bertenaga x-ray dan voltametri kitaran. Pengukuran kuantitatif terhadap peristiwa ikatan antigen spesifik prostat di atas transduser dilakukan menggunakan teknik Spektroskopi Impedans Elektrokimia dalam mod Faradaic (kehadiran spesies redoks) dan mod bukan-Faradaic (tanpa spesies redoks). Pengukuran mod Faradaic dilakukan dengan mengukur perubahan rintangan pemindahan caj di dalam sistem elektrokimia apabila peristiwa ikatan sasaran berlaku, manakala dalam mod bukan-Faradaic, pengesanan dilakukan dengan mengukur perubahan kapasitans dua lapisan. Pengesanan sasaran bio dalam mod Faradaic menghasilkan julat pengesanan linear $5000\ \text{ng/ml}$ ke $0.5\ \text{ng/ml}$ dengan had pengesanan pada $0.377\ \text{ng/ml}$ dengan menggunakan pengesanan Skema 1. Sementara itu, dengan menggunakan Skema 2, pengesanan sasaran mod Faradaic menghasilkan julat pengesanan linear $100\ \text{ng/ml}$ ke $0.01\ \text{ng/ml}$ dan had pengesanan pada $0.01\ \text{ng/ml}$. Dalam mod bukan-Faradaic, julat pengesanan linear yang dihasilkan ialah daripada $5000\ \text{ng/ml}$ ke $0.5\ \text{ng/ml}$ dan had pengesanan pada $0.5\ \text{ng/ml}$. Pengamatan terhadap tahap keboleholangan, kekhususan dan kestabilan alat pengesan

sasaran bio tersebut menunjukkan prestasi yang unggul untuk terus dibangun untuk direalisasikan sebagai platform peranti titik penjagaan yang berkesan.

©This item is protected by original copyright

Label-Free Gold Interdigitated Microelectrodes Immunosensor for Prostate Cancer Biomarker

ABSTRACT

Prostate cancer is a slowly proliferating and non-symptomatic form of malignancy in the prostate gland. It is the second most commonly diagnosed type of cancer worldwide, with 28% deaths among diagnosed cases. Although with an introduction of cancer screening in the last few decades had saved countless lives, this technique could not reach out to the patients who live in rural areas due to its inherent complexities and non-portability. Recent developments in label-free and portable biosensing platforms using the gold-standard prostate-specific antigen are catered towards solving this current diagnoses loophole. Similarly, this research work develops a label-free gold interdigitated microelectrodes immunosensor which target to solve these limitations in the current cancer diagnostic technologies. In this work, an interdigitated microelectrodes architecture is chosen due to its superior detection sensitivity, portability and mass manufacturability. The device is fabricated in-house using an established Complementary Metal-Oxide Semiconductor fabrication process, with a gold microelectrode size of 10 μm and interdigitated gap size of 10 μm , integrated with a gold counter electrode and gold pseudo-reference electrode on a silicon dioxide substrate. For biosensing device development, two transducer surface modification schemes are demonstrated. Scheme 1 involves a self-assembled monolayer modification using amino-silanization of 3-aminopropyltriethoxysilane and immobilization of monoclonal antibody specific to prostate-specific antigen on the silicon dioxide substrate, meanwhile Scheme 2 involves modification of self-assembled monolayer using thiolation chemistry of 16-mercaptoundecanoic acid and immobilization of the monoclonal antibody on gold microelectrode surface. Successful sensor's modification steps are validated using atomic force microscopy, water contact angle measurement, X-ray photoelectron microscopy, and cyclic voltammetry characterization techniques. The binding event of prostate-specific antigen target on device transducer is quantitatively measured using a highly-sensitive Electrochemical Impedance Spectroscopy technique in both Faradaic (in presence of redox species) and non-Faradaic (in absence of redox species) modes of measurement. The Faradaic measurement is performed by measuring the changes in charge transfer resistance in the electrochemical double layer upon target binding, meanwhile in non-Faradaic mode, the detection is made by measuring the changes in the double layer capacitance of the electrochemical system. Using the detection Scheme 1, the bio-detection of prostate-specific antigen in Faradaic mode reveals a linear detection range of 5000 ng/ml to 0.5 ng/ml, with a limit of detection at 0.377 ng/ml. On the other hand, in Scheme 2, Faradaic measurement reveals a linear detection range of 100 ng/ml to 0.01 ng/ml and limit of detection of 0.01 ng/ml. In non-Faradaic mode, linear detection range of 5000 ng/ml to 0.5 ng/ml and limit of detection of 0.5 ng/ml are reported. The sensors' reproducibility, specificity and stability studies reveal highly promising sensing performances that warrant for future development into a point-of-care biosensing platform.

CHAPTER 1 : INTRODUCTION

1.1 Motivation

Since the first sighting on prostate cancer (PCa) by (Adams, 1853), it took the whole 88 years to discover an androgen-ablation therapy by Charles Huggins in 1940s, the first effective treatment to combat this disease. Furthermore, it was not more than only three decades ago since the prostate-specific antigen (PSA) screening was introduced had revolutionized our approach to tackle this endemic fatality. Albeit the long-time taken, these medical discoveries are nothing from the sort of miracles, except from the hard works among the scientists that led to these scientific breakthroughs that had saved countless lives.

There are many interesting effects due to discovery of PSA. For a start, the increase in the number of PCa prognosis from PSA screening is apparent, which translate to greater possibility of lives being saved. This life-saving fact holds true as reported shows the PSA screening has increased the success rate of PCa detection to ~70-80%, that is 50% increased before the use of PSA screening (Catalona, Smith, Ratliff, & Basler, 1993). It was also reported that the combination of PSA screening with digital rectal examination (DRE) test have led to a greater sensitivity in detecting the organ-confined PCa compared to DRE or transrectal ultrasound (TRUS) alone (Brawer et al., 1992; Crawford et al., 1996; Mettlin et al., 1993). Albeit these successes, the current PSA screening method still relies on the time-consuming and complicated laboratory-based tests that prolong the diagnosis time. Other than that, technique such as biopsy poses the risks of internal bleedings and infections, furthermore, not to

mention the psychological effects that lead to embarrassment among the patients. These loopholes have led to hesitation among men to undergo such procedures, resulting in complications to detect PCa in its early stage. Therefore, the principle motivation of this research is to eliminate these diagnostic loopholes by transitioning the existing methods into a label-free, portable, and highly sensitive immunosensing platform for early detection of PCa. The term ‘immunosensing’ describes the application of a sensing platform in this research work that incorporates the highly-specific immuno-response of the immobilized monoclonal antibody (mAb) towards the PSA target antigen.

1.2 Research background

An accurate diagnosis in earlier cancer stage is crucial to yield better disease monitoring and successful treatment for PCa. Many conventional PSA detection methods have been developed, such as, enzyme-linked immunosorbent assay (ELISA) (Matsumoto et al., 1999, 2000), fluorescence immunoassay (Choi et al., 2013), bioluminescent immunoassay (Ito et al., 2007), chemiluminescence immunoassay (Jolly, Damborsky, et al., 2016), and time-resolved fluorescence assay (Härmä et al., 2003; Siivola et al., 2000). Albeit their good sensitivity, these methods are complicated, require labels or tags, laborious, non-portable, time-consuming, and expensive. Another interesting method, the immunochromatography test strip (ICTS) (Li et al., 2014) offers the speed, portability, simplicity and point-of-care (PoC) testing, however it requires high antigen loading to produce translatable output. Furthermore, most of the reported ICTS outputs are of qualitative nature at most, and rarely semi-quantitative.